New Journal of Physics
The open access journal at the forefront of physics

Deutsche Physikalische Gesellschaft DPG IOP Institute of Physics

Broadband generation in a Raman crystal driven by a pair of time-delayed linearly chirped pulses

To cite this article: Miaochan Zhi and Alexei V Sokolov 2008 *New J. Phys.* **10** 025032

New Journal of Physics
The open-access journal for physics

Broadband generation in a Raman crystal driven by a pair of time-delayed linearly chirped pulses

Miaochan Zhi[1] **and Alexei V Sokolov**
Physics Department and Institute for Quantum Studies,
Texas A & M University, College Station, TX 77843-4242, USA
E-mail: mczhi@neo.tamu.edu

New Journal of Physics **10** (2008) 025032 (12pp)
Received 19 October 2007
Published 29 February 2008
Online at http://www.njp.org/
doi:10.1088/1367-2630/10/2/025032

Abstract. A pair of time-delayed linearly chirped pulses with sub-picosecond duration is used to selectively excite Raman transitions in a lead tungstate crystal. Significant molecular coherence leads to generation of up to 40 anti-Stokes and 5 Stokes sidebands. High conversion efficiency (from the two pump beams to the sidebands) is measured. The broadband generation with chirped pulses whose duration is comparable to the Raman coherence lifetime is considerably more efficient, when compared to the case of excitation by two-color femtosecond pulses. In the future, mutual coherence among the generated sidebands may allow ultrashort pulse synthesis.

Contents

[1] Author to whom any correspondence should be addressed.

1. Introduction

In the past, broadband collinear Raman generation in molecular gases has been used to produce mutually coherent equidistant frequency sidebands spanning several octaves of optical bandwidths [1]. It has been suggested that these sidebands can be used to synthesize optical pulses as short as a fraction of a femtosecond (fs) [2]. The technique relies on adiabatic preparation of near-maximal molecular coherence. While at present isolated attosecond x-ray pulses are obtained by high harmonic generation [3], the Raman technique shows promise for highly efficient production of such ultrashort pulses in the near-visible spectral region, where such pulses inevitably express a single-cycle nature and may allow non-sinusoidal field synthesis [2].

We have recently reported broadband generation in lead tungstate ($PbWO_4$), which is a Raman-active crystal; moreover, we have shown that the generated sidebands are mutually coherent [4]. Since coherence lifetime in a solid is typically shorter than in a gas, the use of fs (or possibly picosecond (ps)) pulses is inevitable when one wants to use coherence effects in a room-temperature crystal. Previously, coherent high-order anti-Stokes (AS) scattering (produced by two-color fs pulses) was observed in crystals $YFeO_3$, $KTaO_3$ and $KNbO_3$ [5]–[7], and impulsive Raman scattering was observed in $KGd(WO_4)_2$ crystal [8]. We also note related work on impulsive excitation of phonon modes in molecular crystals by terahertz trains of fs pulses [9].

In our earlier experiments, we used two nearly transform-limited 50 fs laser pulses tuned such that their frequency difference was approximately equal to the Raman frequency. We observed up to 20 AS and 2 Stokes (S) sidebands, covering infrared, visible and ultraviolet spectral regions. One complication in those experiments was simultaneous excitation of several Raman lines by the large spectral width of the fs laser pulses. Also, the high-peak intensity of the pulses leads to generation of strong instantaneous four wave mixing (FWM) signals. These result in a rich structure of the lower-order sidebands' spectra. In addition, the total laser energy fluence in those experiments was limited by 'parasitic' nonlinear processes, such as self-focusing and self-phase-modulation (SPM), which can strongly distort the pulses.

Femtosecond pulse sequencing and shaping allows selective (narrow-band) Raman excitation by broadband pulses, as discussed in the past [10]–[12]. At the same time, the shaped pulses are necessarily longer than transform-limited, and therefore have lower peak intensity, helping to avoid the onset of parasitic nonlinear processes at larger energy fluences.

In this paper, we study the broadband generation in lead tungstate pumped by a pair of time-delayed linearly chirped pulses. While the transform-limited pulse duration is 35 fs, the chirped pulse duration ranges from 100 fs to 2 ps (ideally, one may want to have the shaped pulse duration roughly match the Raman coherence lifetime). For a pair of chirped pulses, the difference between the instantaneous frequencies depends only on the relative pulse delay. When this frequency difference equals a Raman frequency, a periodic pulse train is created in the time domain, with a period equal to the period of a single Raman vibrational mode. As a result, this Raman mode can be selectively excited [10]. A simplified set-up for high-resolution spectroscopy has been built using a pair of time-shifted, linearly chirped pulses [11]. A related method of achieving the spectral selectivity is Fourier domain pulse shaping, where a pulse train is created by applying a periodic spectral phase to a single fs pulse using a pulse shaper [12].

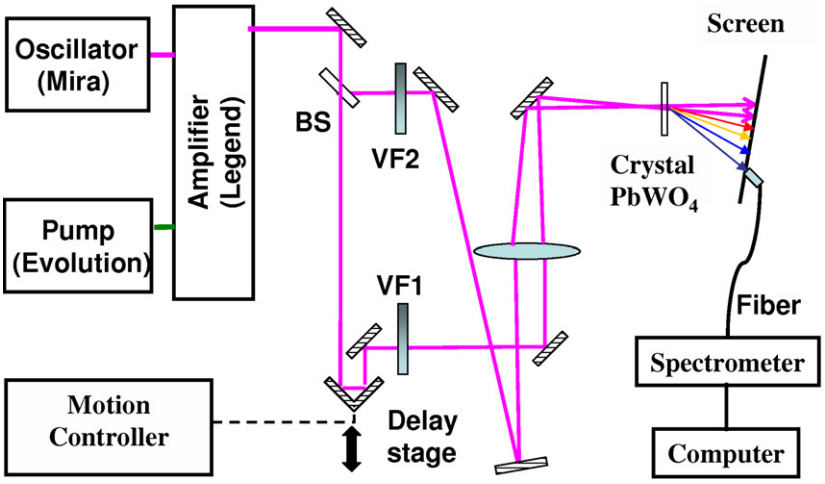

Figure 1. Schematic of the experimental set-up. VF: variable neutral density filter; BS: 50/50 ultrafast beamsplitter. An approximately linearly chirped pulse is obtained by misalignment of the compressor in the amplifier. The amplified output pulse is split into two and later recombined at the sample with a relative time delay.

2. Experimental set-up

Our experimental set-up is shown in figure 1. Briefly, the output of the regenerative amplifier (legend, coherent) is an infrared beam ($\lambda = 802\,\text{nm}$) of 35–50 fs pulses with a 1 kHz repetition rate and 1 W average power. Before amplification, the oscillator pulses are chirped by a pulse stretcher (which is a part of the amplifier system). After amplification, the pulses are sent through a compact compressor (in a folded geometry). This compressor works with just one diffraction grating, and a roof-top mirror is used to reflect the beam back to the (same) grating. A long pulse with a frequency chirp is compressed by this device to a short pulse with no chirp. The roof-top mirror is mounted on a motorized translation stage. Translation of the roof-top mirror results in a change of the distance that the pulse travels from the grating to the mirror and back, and the chirp of the output pulse also changes. The pulse is then split into two by an ultrafast beamsplitter. The delay between the two pulses can be varied by moving a retroreflector which is mounted on a motorized translation stage (with electronic motion control). The two beams are recombined and focused in the crystal by a 2 in diameter lens (focal lens $f = 50\,\text{cm}$). Both beams are attenuated by variable neutral density filters so that the power used is below the threshold for the parasitic nonlinear processes. The power used ranges from 5 to 20 mW, depending on the pulse chirp and the focusing conditions. Figures 2(a) and (b) show schematic and measured chirped pulses as applied to our sample.

The Raman-active crystal of our choice (lead tungstate, $PbWO_4$) exhibits good optical transparency, high damage threshold, and is non-hygroscopic. $PbWO_4$ has a strong narrow Raman line at $903\,\text{cm}^{-1}$ with linewidth $\Delta\nu_R = 4.3\,\text{cm}^{-1}$, which corresponds to a phonon relaxation time $T_2 \approx 2.5\,\text{ps}$ [13]. Another relatively strong Raman line at $325\,\text{cm}^{-1}$ has a coherence lifetime of 1.5 ps. Our sample is 1 mm thick, and the laser beams are typically sent perpendicular to its surface and parallel to the crystalline a-axis.

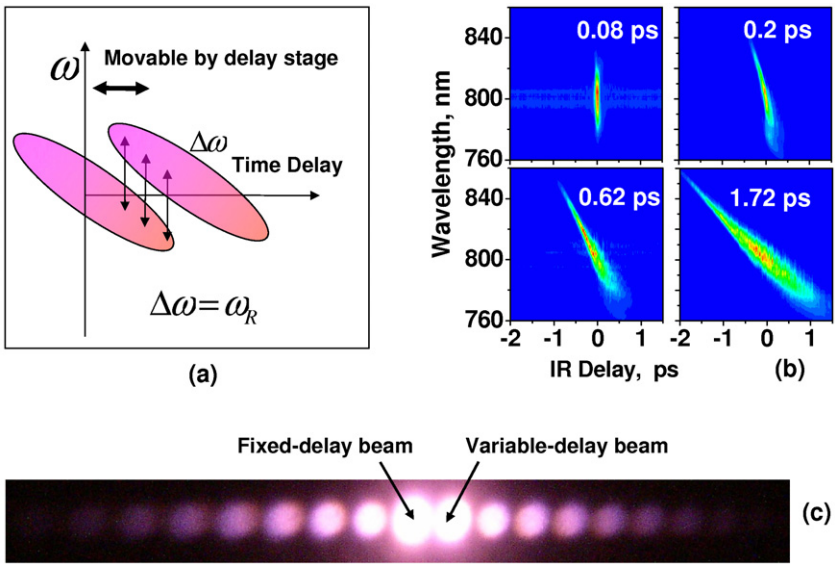

Figure 2. (a) The schematics of the (chirped and time-delayed) pulses used for selective Raman excitation. When the instantaneous frequency difference between a pair of chirped pulses equals a Raman frequency, this Raman mode can be selectively excited. (b) The pulse chirp measured with the SD-FROG method. The chirped pulse duration is given in each plot. We introduce chirp to a near-transform-limited pulse (top left) and obtain pulses with chirp rate 1280 (top right), 620 (bottom left), 320 (bottom right) $cm^{-1}\,ps^{-1}$, respectively. (c) Multiple orders of beam cross-diffraction produced by the two pulses crossed in the $PbWO_4$ at zero delay.

The zero delay between the two pump pulses can be found by focusing the two beams (unchirped pulses) at a very small (less than 2°) crossing angle in a piece of glass. When the two beams overlap both in space and time, an interference pattern around the two pump beams can be easily seen by eye, when the beams are projected on to a paper screen placed behind the crystal. Several orders of beam cross-diffraction can be seen when enough power is applied. Since the two pulses used in this experiment are identical, the observed effect is commonly referred to as self-diffraction (SD). The diffracted beams show up symmetrically beside the two pump beams, as shown in figure 2(c). Note here the set-up is the same as that is used in SD-frequency-resolved optical gating (SD-FROG) to characterize a short pulse [14]. We use the first-order diffracted beam next to the pump beam with a variable delay, in order to measure the chirp produced at the output of the amplifier system. The measurement results are shown in figure 2(b). The pulse that is used here is negatively chirped, with a pulse duration full width at half maximum (FWHM) ranging from 80 fs to 2 ps. The chirp is approximately linear. The narrowing of the spectrum on the top (longer wavelength) may be due to the limited measuring range of the fiber-coupled spectrometer, which cuts off at 870 nm wavelength and has a reduced sensitivity just below that. The multiple cross-diffraction beams produced in lead tungstate (figure 2(c)) are much stronger compared to those produced in, for example, glass.

3. Chirped pulse basics

If a transform-limited pulse is sent through a pulse stretcher/compressor, its duration increases (due to pulse chirping) proportionally to the distance l between the gratings, as given by [15]:

$$\delta_\lambda \tau = \frac{l(\lambda/d)\delta\lambda}{cd[1-(\lambda/d-\sin\gamma)^2]}, \tag{1}$$

where $\delta_\lambda \tau$ is the variation of group delay, l is the slant distance between the gratings, d is the grating constant, $\delta\lambda$ is the bandwidth of the pulse, c is the speed of light, and γ is the angle of incidence. In our experiment, $\lambda = 802\,\text{nm}$, $\delta\lambda = 35\,\text{nm}$, $d^{-1} = 1500\,\text{lines mm}^{-1}$ and γ is about 30°. Plugging in these numbers we get: $\delta_\lambda \tau = 4.2\,l\,\text{ps cm}^{-1}$.

In terms of frequency $\omega(=2\pi c/\lambda)$, the group delay can be expressed as:

$$\delta_\omega \tau = \frac{-4\pi^2 cl\delta\omega}{\omega^3 d^2[1-(\lambda/d-\sin\gamma)^2]}. \tag{2}$$

Thus, the time delay of a spectral component at a frequency ω can be expressed as [15]:

$$\tau = \tau_0 - \frac{\omega-\omega_0}{\mu} + O(\omega-\omega_0)^2. \tag{3}$$

Therefore, the relative delay is (to the first order) proportional to the frequency difference:

$$\Delta\tau = t_\text{d} = \Delta\omega/\mu.$$

Here,

$$\mu^{-1} = -4\pi^2 cl/\{\omega^3 d^2[1-(\lambda/d-\sin\gamma)^2]\}.$$

We see for fixed $\Delta\omega$, t_d is proportional to l. t_d is also proportional to the inverse of the pulse chirp, as is shown next.

A linearly chirped pulse can be written as:

$$E(t) = \exp(-at^2) \times \exp[I \times (bt^2 + \omega_l t)]. \tag{4}$$

Here, $1/\sqrt{a}$ is roughly the pulse duration, b is the chirp rate of the pulse and ω_l is the laser center frequency.

The intensity for two time-delayed linearly chirped pulses is:

$$\begin{aligned} I(t) &= |E(t) + E(t-t_\text{d})|^2 \\ &= \exp(-2at^2) + \exp[-2a(t-t_\text{d})^2] + 2\exp[-a(t^2+(t-t_\text{d})^2]\cos[b(2t-t_\text{d})t_\text{d} + \omega_l t_\text{d}]. \end{aligned} \tag{5}$$

When $\Delta\omega = \omega_\text{R} = bt_\text{d}$, the last term in I_t is proportional to $\cos(2\omega_\text{R}t + C)$ ($C = (\omega_l\omega_\text{R} - \omega_\text{R}^2)/b$, is a constant). We see that there is a periodic beat in the pulse intensity in the time domain. The periodicity of this pulse train can be matched to the period of this Raman mode at ω_R, permitting selective mode excitation [11]. One can adjust the excitation frequency simply by adjusting the time delay between the two pulses.

We change the chirp gradually by a controller. Assuming a linear chirp, for three different settings of the controller we measure a chirp rate of 1281, 620, and 320 $\text{cm}^{-1}\,\text{ps}^{-1}$, respectively (figure 2(b)). For a fixed $\Delta\omega = \omega_\text{R}$, t_d is proportional to $1/b$, so the slope of t_d versus the inverse of the chirp rate gives the Raman frequency ω_R (which is to be excited). We calculate the chirp rate b from $b = \omega_\text{R}/t_\text{d}$ by measuring the t_d using pulses with different chirp rate when the Raman

mode at 325 cm^{-1} is excited. We find these chirp rates agree well with our direct measurements using the SD-FROG method, which justifies our assumption of a linear chirp.

Molecular vibrations resonantly excited by a periodic sequence of short pulses have been described in detail by Zheltikov [10] and Gershgoren *et al* [11]. Our own interest in this area comes from a possibility of producing multiple orders of coherent Raman sidebands, as a result of the strongly excited molecular vibrations, similar to the Raman sideband generation in molecular gases [1].

4. Experimental results and discussion

In the present work, we concentrate on optimizing the generation of a broad spectrum of coherent Raman sidebands, and study the opportunities offered by selective excitation of three distinct Raman modes in lead tungstate. We have previously shown that the angle between the two pump beams is very critical for sideband generation in Raman crystals [4]. For example, to effectively excite the 903 cm^{-1} Raman mode (in lead tungstate), an angle of 3°–4° is needed, while for the lower frequency Raman mode at 325 cm^{-1} to be excited, a smaller angle of 2.5° works the best. We vary the angle by adding an $f = 20$ cm negative lens after the $f = 50$ cm lens and adjust the distance between the lens. In the following part of this paper, we discuss the sideband generation at different crossing angles between the two pump beams. For convenience of description, we call the pump beam with variable pulse delay the variable-delay pump and the other one the fixed-delay pump beam.

4.1. Broadband generation by a coherently excited 191 cm^{-1} Raman mode

We apply two collimated pump beams (beam size about 1 mm) crossed at 1.2° angle, to the $PbWO_4$ crystal. We use linearly chirped pulses with a chirp rate of 2100 cm^{-1} ps^{-1}. At zero relative pulse delay, we observe beam diffraction similar to what is shown in figure 2(c). When we adjust the pulse delay to $t_d = 0.087$ ps, we observe up to 40 AS and 5 S sidebands generated as shown in figure 3(a). We observe AS generation on the variable-delay pump side at a positive pulse delay (here the variable-delay pump acts as the pump beam and the fixed-delay pump acts as the Stokes beam, as conventionally $\omega_{pump} > \omega_{Stokes}$). When we move the pulse forward from 0 delay to $-t_d$, we observe AS generation on the side of the fixed-delay pump beam (as expected), since now the fixed-delay beam functions as a pump beam. In these experiments, as well as in most of the previously described experiments on molecular modulation in gasses and solids, we observe a larger number of AS sidebands than Stokes ones. This asymmetry is typically present since the Raman frequency is only one or two orders of magnitude smaller than the laser frequency, and hence the total generated bandwidth is comparable to the pump laser frequency. At substantially lower frequencies generation is intrinsically less efficient. In addition, infrared sidebands are harder to detect. Finally, in the present experiment (as shown in figure 3) phase matching occurs at a considerably larger output angle (and leads to a correspondingly worse spatial overlap with the pump beams) for a Stokes sideband compared to the same order AS sideband.

The substantial pulse chirping, as well as the relatively loose beam focusing, allow us to use a rather high combined average power of over 15 mW (measured after the crystal). We observe highly efficient frequency-sideband generation, with both applied beams depleted by 25% due to energy conversion into the generated sidebands. In figure 3 (bottom)

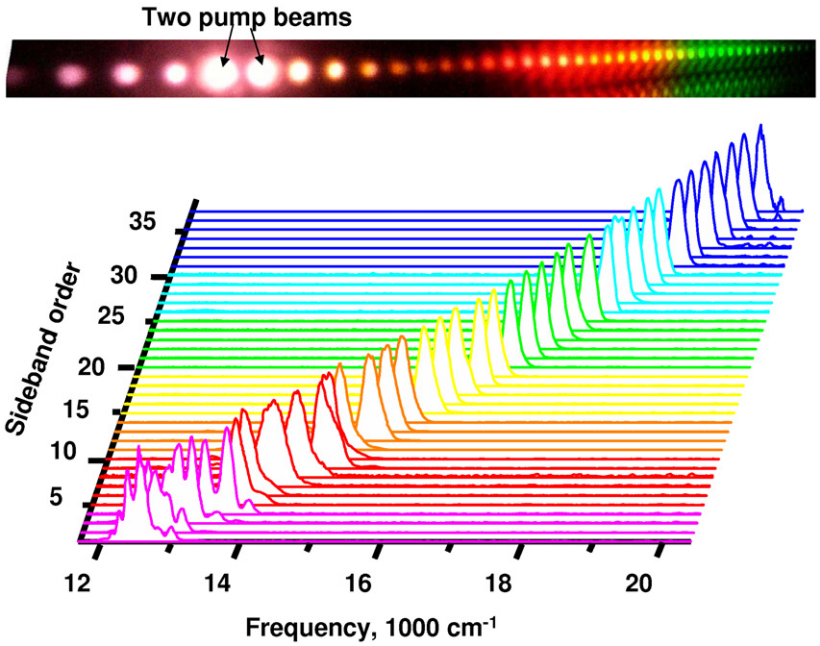

Figure 3. Broadband generation in a $PbWO_4$ crystal using two time-delayed linearly chirped pulses, with the chirp rate of 2100 cm^{-1} ps^{-1} and relative pulse delay of 0.087 ps. The two applied beams crossed at an angle of 1.2°. Top: the generated beams projected on to a white screen. Bottom: normalized spectra of the generated sidebands from AS 1 to AS 37.

we show the normalized spectra of the generated sidebands (from AS 1 to AS 37). There is substantial overlap between the spectra of the generated sidebands. When the angle is smaller and therefore a lower-frequency Raman transition is excited, we observe continuum generation instead of the distinctive spots for the high-order sidebands, due to the small angle separation and the wide spectrum of the sideband, similar to the picture shown in figure 4(a). From figure 3 (bottom) we measure an average frequency spacing of 200 cm^{-1} for the generated sidebands. We believe the generation at this angle is due to the excitation of the 191 cm^{-1} Raman line. This can also be verified by calculating the Raman frequency using $\omega_R = bt_d = 183\,cm^{-1}$.

4.2. Broadband generation by a coherently excited 325 cm^{-1} Raman mode

When two-color excitation is used and the angle between the two pump beams is small, we observe the generation due to 325 cm^{-1} Raman mode excitation. About 22 AS sidebands are observed as shown in figure 4(a); however, only 2–3 mW of average beam power can be used, limited by the onset of the SPM. This mode should be easily accessed by the pair of identical time-delayed chirped pulses, since the available spectral width (FWHM) of the pulse is around 460 cm^{-1}. To observe this, we use one 2 in lens with a focal length of 50 cm. The resultant angle between the pump beams is about 2.4°. We observe as many as 40 AS at two different delays. The output angle of the highest-order sideband with respect to the pump beam is about 80°.

When we change the pulse chirp to 620 cm^{-1} ps^{-1}, we observe, unexpectedly, that some of the high-order sidebands are stronger than the low-order ones, as shown in figure 4(d). This

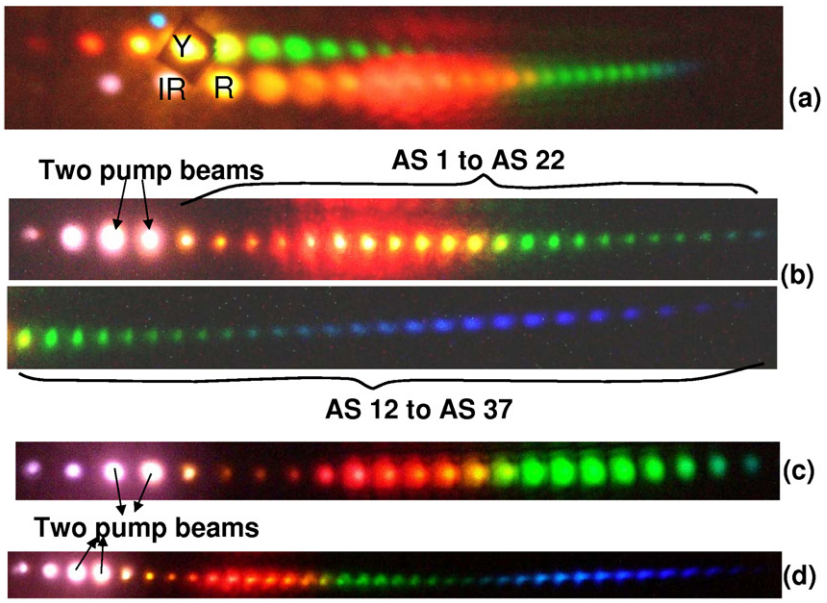

Figure 4. (a) Broadband generation in $PbWO_4$ pumped by nearly-transform-limited fs pulses (IR, $\lambda_{\text{Stokes}} = 804\,\text{nm}$ and R, $\lambda_{\text{pump}} = 766\,\text{nm}$). The angle between the pump and Stokes beams is 2.9°. A third probe pulse (Y) leads to the generation of many orders of S and AS sidebands. (b) and (c) Broadband generation in $PbWO_4$ using two time-delayed linearly chirped pulses applied at an angle of 2.4° to each other. The pulse chirp is about $1280\,\text{cm}^{-1}\,\text{ps}^{-1}$ for (b), and $440\,\text{cm}^{-1}\,\text{ps}^{-1}$ for (c). (d) The intensity modulation of the generated sidebands is clearly seen when the pulse chirp is about $620\,\text{cm}^{-1}\,\text{ps}^{-1}$.

can be seen even more clearly when a larger angle between the two pump beams is used and when the Raman mode at $903\,\text{cm}^{-1}$ is excited (as described below). Inoue *et al* [16] have observed a similar non-monotonic variation of spectral intensity of the generated sidebands when using two-color sub-ps excitation in TiO_2 crystal. There are two possible explanations of this non-monotonic dependence of the generation efficiency on the sideband order. One possible explanation is based on our experimental observation. Since the FWM coexists with the Raman process, certain sidebands get enhanced when the two processes overlap at that order (see figures 6(a) and (b)). Another potential mechanism for the observed effect may be related to the dynamics of laser–crystal interaction. Our preliminary theoretical calculation shows that the intensity modulation of the generated spectrum might be due to non-adiabatic behavior of the system, determined by an interplay of pulse durations, the Rabi period and the dephasing time for the Raman transition [17]. Further investigation is needed in order to explain this observation.

Broadband generation at a chirp rate of $1280\,\text{cm}^{-1}\,\text{ps}^{-1}$ and a pulse delay of 0.7 ps are shown in figure 4(b). We observe 40 AS and 3 S sidebands. The frequency separation between the sidebands is around $320\,\text{cm}^{-1}$ on average. It decreases to $240\,\text{cm}^{-1}$ for the high-order sidebands.

We measure high nonlinear conversion efficiency. As much as 41% of the pump pulse energy and 21% of the Stokes pulse energy are converted into the generated sidebands. When the chirp rate is increased to $1060\,\text{cm}^{-1}\,\text{ps}^{-1}$, the sideband generation seems to become less

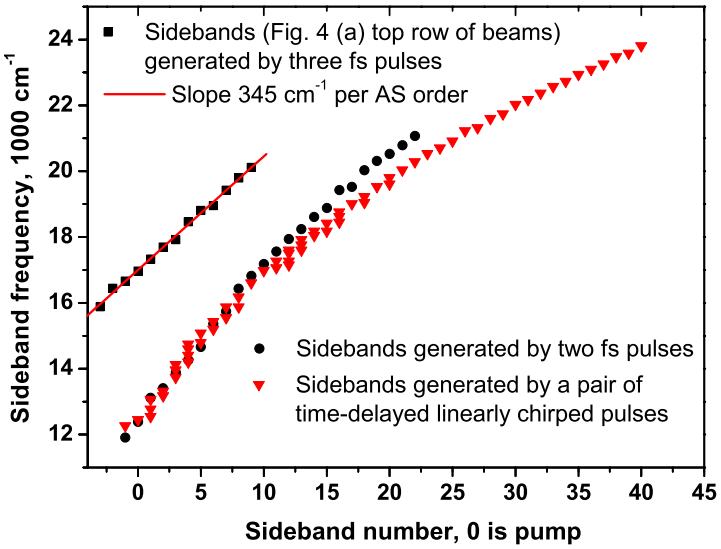

Figure 5. Comparison of the sideband generation in $PbWO_4$ using two nearly-transform-limited fs pulses ($\lambda_{Stokes} = 804$ nm and $\lambda_{pump} = 766$ nm) and a pair of time-delayed chirped pulses. Many more sidebands are generated in the latter case.

effective. The number of observed AS sidebands decreases to 34. The conversion efficiency from the pump and Stokes beams decreases to 33 and 19%, respectively. When we introduce more chirp until a chirp rate of 440 cm^{-1} ps^{-1} is reached, the efficiency reduces to about 14% for the pump and 11% for the Stokes beam. About 22 AS sidebands are observed. However, the absolute input power can be increased to 15 mW without introducing the parasitic effects. Another feature of the generation using pulses with a high chirp rate is that the FWM signal gets weaker. Consequently, the generated sidebands have good beam profiles, as shown in figure 4(c), and their spectra are mostly single-peaked.

In figure 5, we plot the sideband frequency as a function of the sideband order. The squares show the peak frequencies of the sidebands generated by all three beams when fs pulses are used (as in figure 4(a), top row of beams). The probe beam (yellow) is labeled as 0 order. The frequency spacing is regular, about 345 cm^{-1} per AS order. Compared to the sidebands generated by two (nearly-transform-limited) fs pulses (figure 5, filled circles), there are many more sidebands generated when a pair of time-delayed linearly chirped pulses are used (figure 5, triangles). The AS sidebands span a range of 12 000 cm^{-1}.

4.3. Broadband generation by a coherently excited 903 cm^{-1} Raman mode

We also observe the sideband generation due to the excitation of the Raman mode at 903 cm^{-1}, the strongest Raman mode in the $PbWO_4$ crystal, although the FWHM of the pulse, we used is around 400–500 cm^{-1}. We use an angle between the two pump beams of about 4°. We observe generation of up to 19 AS sidebands, as shown in figure 6.

With a large angle, the non-resonant FWM signal is more separated from the Raman generation as shown in figure 6(a). We show the sideband generation picture at three consecutive time delays between the two pump beams, with a separation of 33 fs. As we can see, the large

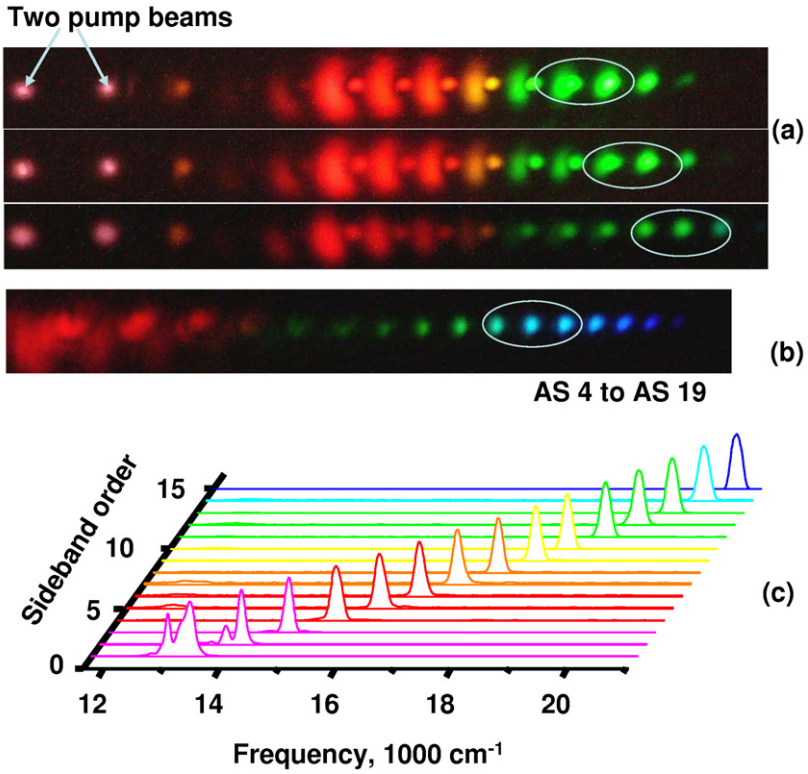

Figure 6. Sideband generation in $PbWO_4$ using two time-delayed linearly chirped pulses applied at an angle of 4° to each other. The pulse chirp is about 620 cm^{-1} ps^{-1}, and the pulse delay is about 1.43 ps. (a) The generated beams projected onto a white screen. Pictures are taken at three consecutive time delays between the two pump beams, with an increase of 33.3 fs. (b) The picture of the high-order sidebands. They are brighter than the low-order sidebands. (c) Normalized spectra of the generated sidebands (AS 1–AS 15). The frequency spacing of the high-order sidebands is around 540 cm^{-1} per AS order.

spot, which is due to FWM generation process, shifts as the delay varies. When a certain order (circled by dots in figure 6(a)) overlaps with the Raman generation (small round spot), the intensity of that order is enhanced. When lower power or higher-chirp rate pulses are used, the FWM process weakens and only sidebands generated through Raman processes appear. When high power or less-chirped pulses are used, the FWM process sometimes leads to the distorted beam profile of the lower orders due to the competition between the two processes as shown in figure 6(b). However, the high-order sidebands have good beam profiles. The spectra of the generated sidebands are shown in figure 6(c). The frequency spacing between the sidebands is decreasing from low-order to high-order sidebands, similar to what we have observed for sideband generation using the two-color fs excitation [4].

The sideband generation in the crystal is strongly influenced by the phase matching and thus the sidebands have a varying frequency spacing (decreasing for high-order sidebands). When we plot the sideband peak frequency as a function of the sideband order, we see a linear slope with 540 cm^{-1} per AS order. There are several Raman modes in $PbWO_4$ crystal [13]. When we plot t_d as a function of $1/b$, we obtain a linear slope of 923 cm^{-1}. Therefore, we

confirm the excitation of the 903 cm^{-1} Raman mode. For small angles, we measure a slope of 340 cm^{-1}, which confirms the excitation of the 325 cm^{-1} Raman mode.

5. Conclusions and implications

We observe the efficient generation of multiple frequency sidebands in lead tungstate driven by a pair of chirped pulses. We adjust the chirp so that the pulse duration is close to the coherence lifetime in this Raman-active crystal. Temporal stretching of the excitation pulses allows us to use large pulse energies per unit area (while still avoiding parasitic nonlinear effects), and correspondingly increase the Raman coherence. In order to optimize the generation process, we study the effect of time delay (or the pulse chirp rate), and the crossing angle between the two pump beams, on the efficiency of sideband generation. We measure up to 40 AS and 5 S sidebands generated when a Raman mode at 190 cm^{-1} is resonantly excited. In this case, the conversion efficiency from the two pump beams into the sidebands is high; for example, we have measured as high as 41% conversion efficiency for the pump beam and 21% for the Stokes beam. Similarly to the case of two-color fs pulse excitation (when the frequency separation between the pulses is close to the Raman frequency), we expect the generated sidebands to be mutually well-coherent. Compared to the fs excitation, we observe more sidebands generated by the chirped pulses (the AS sidebands cover a range of 12 000 cm^{-1} span). Although the FWM process still creates some multiple peaks in the spectra of the low-order sidebands, the complications due to simultaneous excitation of multiple Raman lines are eliminated. Different Raman modes can be selectively excited by varying the time delay and the angle between the two pump beams. Our experiment confirms that phase matching plays an important role in the Raman generation process.

In the near future, we envision driving one of these Raman transitions by a pair of time-delayed chirped ps pulses, and then using another (compressed or shaped) fs pulse from the same source laser, to probe the Raman coherence prepared by the two excitation pulses. Our experiment has already shown efficient spectral broadening of a (third) probe pulse; future experiments will possibly lead to substantial pulse compression in the same medium, as predicted in our earlier work [1, 2].

Acknowledgments

This project is supported by the National Science Foundation (grant # PHY-0354897), the Defense Advanced Research Projects Agency, an Award from Research Corporation, and the Robert A Welch Foundation (grant # A1547).

References

[1] Sokolov A V and Harris S E 2003 Ultrashort pulse generation by molecular modulation *J. Opt. B: Quantum Semiclass. Opt.* **5** R1

[2] Sokolov A V, Shverdin M Y, Walker D R, Yavuz D D, Burzo A M, Yin G Y and Harris S E 2005 Generation and control of femtosecond pulses by molecular modulation *J. Mod. Opt.* **52** 285

[3] Kienberger R *et al* 2004 Atomic transient recorder *Nature* **427** 817

[4] Zhi M and Sokolov A V 2007 Broadband coherent light generation in a Raman-active crystal driven by two-color femtosecond laser pulses *Opt. Lett.* **32** 2251–3

[5] Takahashi J 2004 Generation of a broadband spectral comb with multiwave mixing by exchange of an impulsively stimulated phonon *Opt. Express* **12** 1185
[6] Matsubara E, Inoue K and Hanamura E 2006 Dynamical symmetry breaking induced by ultrashort laser pulses in $KTaO_3$ *J. Phys. Soc. Japan* **75** 024712
[7] Matsuki H, Inoue K and Hanamura E 2007 Multiple coherent anti-Stokes Raman scattering due to phonon grating in $KNbO_3$ induced by crossed beams of two-color femtosecond pulses *Phys. Rev.* B **75** 024102
[8] Grabtchikov A S, Chulkov R V, Orlovich V A, Schmitt M, Maksimenko R and Kiefer W 2003 Observation of Raman conversion for 70-fs pulses in $KGd(WO_4)_2$ crystal in the regime of impulsive stimulated Raman scattering *Opt. Lett.* **28** 926
[9] Weiner A M, Leaird D E, Wiederrecht G P and Nelson K A 1991 Femtosecond multiple-pulse impulsive stimulated Raman scattering spectroscopy *J. Opt. Soc. Am.* B **8** 1264
[10] Zheltikov A M 2002 Spectroscopic and quantum-control aspects of ultrashort-pulse synthesis through impulsive high-order stimulated Raman scattering *J. Raman Spectrosc.* **33** 112
[11] Gershgoren E, Bartels R A, Fourkas J T, Tobey R, Murnane M M and Kapteyn H C 2003 Simplified setup for high-resolution spectroscopy that uses ultrashort pulses *Opt. Lett.* **28** 361–3
[12] Dudovich N, Oron D and Silberberg Y 2002 Single-pulse coherently controlled nonlinear Raman spectroscopy and microscopy *Nature* **418** 512
[13] Kaminskii A A *et al* 1999 Properties of Nd^{3+} doped and undoped tetragonal $PbWO_4$, $NaY(WO_4)_2$, $CaWO_4$, and undoped monoclinic $ZnWO_4$ and $CdWO_4$ as laser-active and stimulated Raman scattering-active crystals *Appl. Opt.* **38** 4533
[14] DeLong K W, Trebino R and Kane D J 1994 Comparison of ultrashort-pulse frequency-resolved-optical-gating traces for three common beam geometries *J. Opt. Soc. Am.* B **11** 1595
[15] Treacy E B 1969 Optical pulse compression with diffraction gratings *IEEE J. Quantum Electron.* **5** 454
[16] Inoue K, Kato J, Hanamura E, Matsuki H and Matsubara E 2007 Broadband coherent radiation based on peculiar multiple Raman scattering by laser-induced phonon gratings in TiO_2 *Phys. Rev.* B **76** 041101
[17] Burzo A M private communication